Event-Based Field Modeling

M. G. Henderson
Los Alamos National Laboratory,

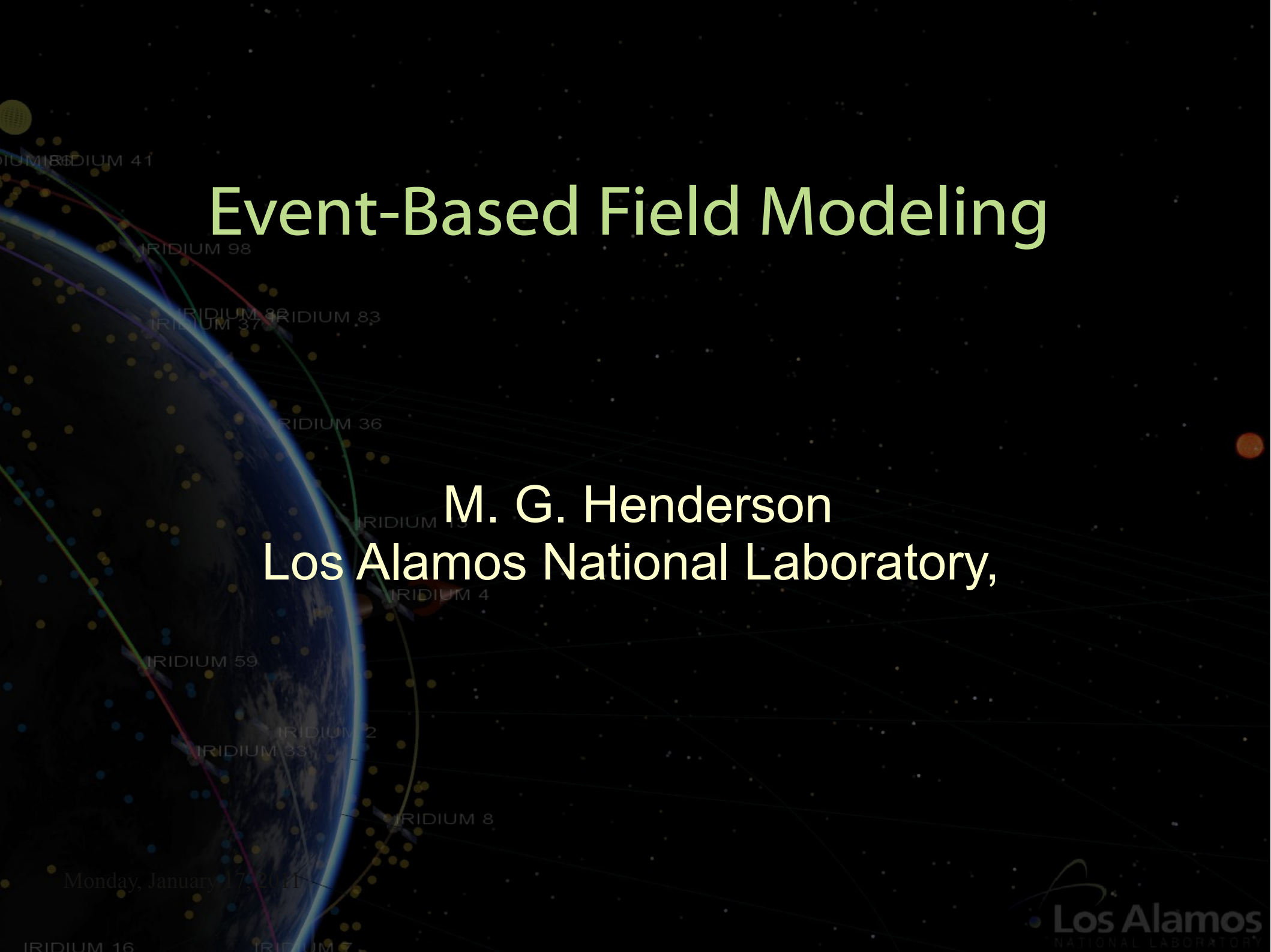

Empirical Field Models

- Functional representation of B-field produced by the various magnetospheric current systems. E.g. tail current, ring current, MP current, Birkeland, etc...
- These models typically have many free parameters associated with each of the current systems.
- Model parameters are determined by fitting to a large set of historical observations.

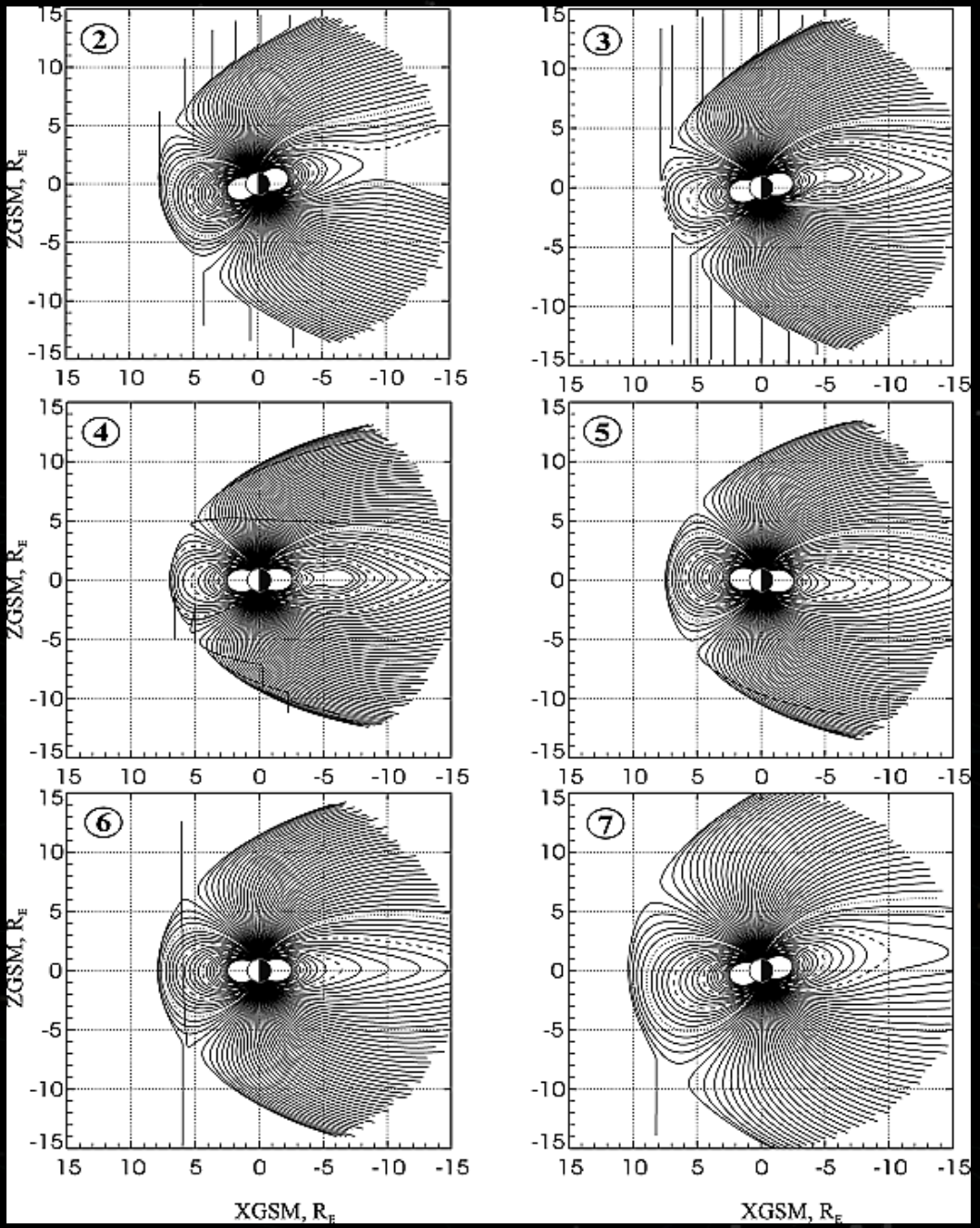

Pros

- Provides excellent average description of the B-field.
- Easily computed with readily available inputs – Kp, Dst, Pdyn, Qin-Denton parameters, etc.
- Models often (though not always) valid over large domain.
- Standard models – everyone knows what `TS04 with Qin-Denton inputs' means.

Cons

- Never really describes B-field accurately for any given event.
- The functional forms may not even be capable of representing the real field.
- Typically only fitted with vector field data – i.e. no mapping (or other) constraints imposed.
- Poorly specified dependence on time history (with the exception of TS07?) Substorms poorly modeled.
- Extreme events poorly reproduced. (E.g. storms, sawtooth events, SMCs, etc.)

Event-Oriented Modeling

- The basic idea is to `tune` existing models to fit the observed conditions for a given event.
- A number of approaches have been used over the years.

Choosing the Best Model

- Many of the early empirical field models were parametrized by Kp – which actually resulted in a set of models. For example, T89c is really a set of 7 different models – each describing a different level of magnetospheric disturbance as indicated by Kp.
- For any individual event there is no guarantee that the best model is the one indicated by the current Kp level.
- This was recognized early on, and it was reasonably common to use whichever model gave the best fit to available field observations. E.g.:
  - Sergeev and Lennartsson, *Planet. Space Sci.*, 36, 4, 353, 1988. The Kp=2 variant of the TU82 model "gave a best fit to observations."
  - Sergeev *et al., Planet. Space Sci., 39, 8,* 1083, 1991. Similar approach with T89 model.

Fitting Input Parameters

- Later models take more input parameters that depend continuously on solar wind conditions (Pdyn, IMF) and geomagnetic indices (e.g. Dst).
- Better matches to data can often be obtained by fitting the input parameters so that the model agrees more closely with observations. E.g;
  - Kubyshkina et al., Magnetospheric currents during sawtooth events, J. Geophys. Res., 113 A08211, doi:1029/2007JA012983, 2008.
  - Kubyshkina et al., Toward adapted time-dependent magnetospheric models: A simple approach based on tuning the standard model, J. Geophys. Res., 114, A00C21, doi:10.1029/2008JA013547, 2009.

Modifying the Models

- Sergeev *et al.*, "Current Sheet Thickness in the Near-Earth Plasma Sheet During Substorm Growth Phase", *J. Geophys. Res.*, 95, A4, 7609, 1990.

  Starting with the T87 model, they made a number of parameters adjustable, added a separate scaling for the tail field, introduced a spatial dependence for the the current sheet thickness, and modified the neutral sheet geometry :

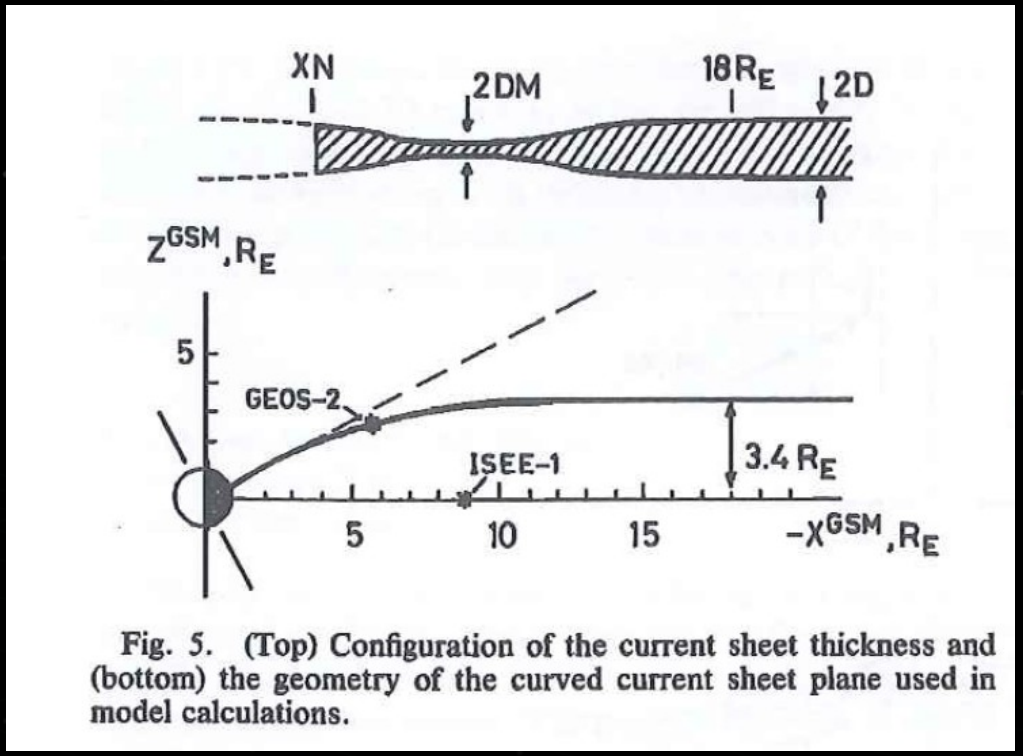

Fig. 5. (Top) Configuration of the current sheet thickness and (bottom) the geometry of the curved current sheet plane used in model calculations.

$$B = B_{CF} + B_{RC}(DR, \rho_0) + f\, B_T(XN, D, DM)$$

$$D(x) = 0.5(D + DM + (D - DM)\cos(2\pi(x/18 + 1)))$$

Modifying the Models

- Intensity and location of the ring current field was adjusted for the event (not fitted). Kp, f, D, DM, XN (inner edge of tail current sheet) were optimized to fit ISEE-1 and GOES-2 field observations.
- Allowed for (presumably) more accurate specification of field configuration at the end of substorm growth phase.

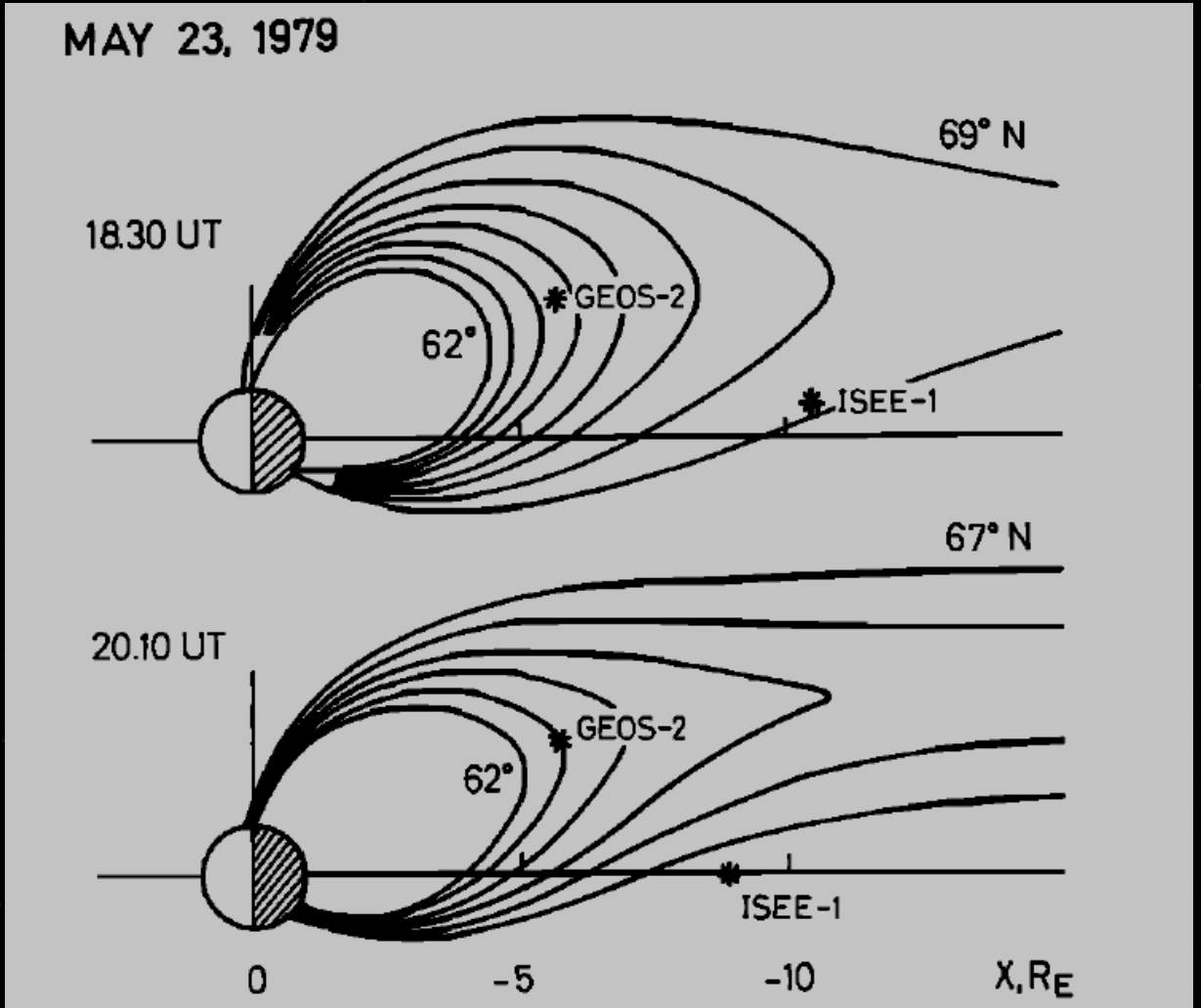

Fig. 7. Magnetic field configurations in the midnight meridional plane at the beginning and at the end of the growth phase of the May 23, 1979, substorm.

Modifying the Models

- Sergeev *et al.*, "Testing the isotropic Boundary Algorithm Method to Evaluate the Magnetic Field Configuration in the Tail", *J. Geophys. Res.*, 98, A5, 7609, 1993.

  Similar approach using T89. Tail current scaled separately (no other modifications.)

  Mapping results used to test the IBA (Isotropic Boundary Algorithm) which hypothesized that equatorward boundary of the isotropic proton precipitation maps to the boundary separating adiabatic and chaotic regimes in the tail.

Time-Dependent Modifications: Growth Phase Modeling

- Pulkkinen *et al.*, Modeling the growth phase of a substorm using the Tsyganenko model and multi-spacecraft observations: CDAW-9", *Geophys. Res. Lett.*, 18, 11, 1963, 1991.
- Pulkkinen *et al.*, Particle Scattering and current sheet stability in the geomagnetic tail during the substorm growth phase, *J. Geophys. Res.*, 97, A12, 19283, 1992.

T89 model used as a starting point. Night-side tail current sheet thinned locally, tail, closure and ring currents are all intensified. And an additional thin-current sheet model is added. A number of parameters are made adjustable and a linear time-dependence is included on a number of the parameters in order to model the evolution of the field during growth phase.

Growth-Phase Modeling

Data-model comparison

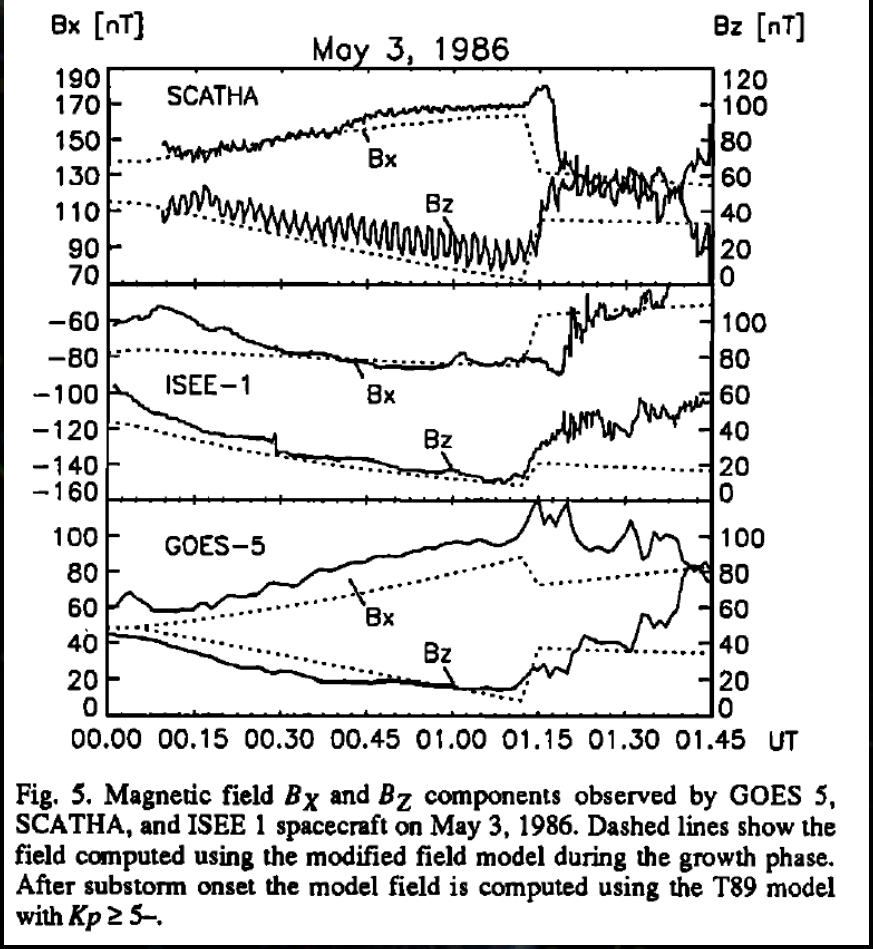

Fig. 5. Magnetic field B_X and B_Z components observed by GOES 5, SCATHA, and ISEE 1 spacecraft on May 3, 1986. Dashed lines show the field computed using the modified field model during the growth phase. After substorm onset the model field is computed using the T89 model with $Kp \geq 5$–.

Pulkkinen *et al.*, *J. Geophys. Res.*, 97, A12, 19283, 1992.

Resulting field configurations

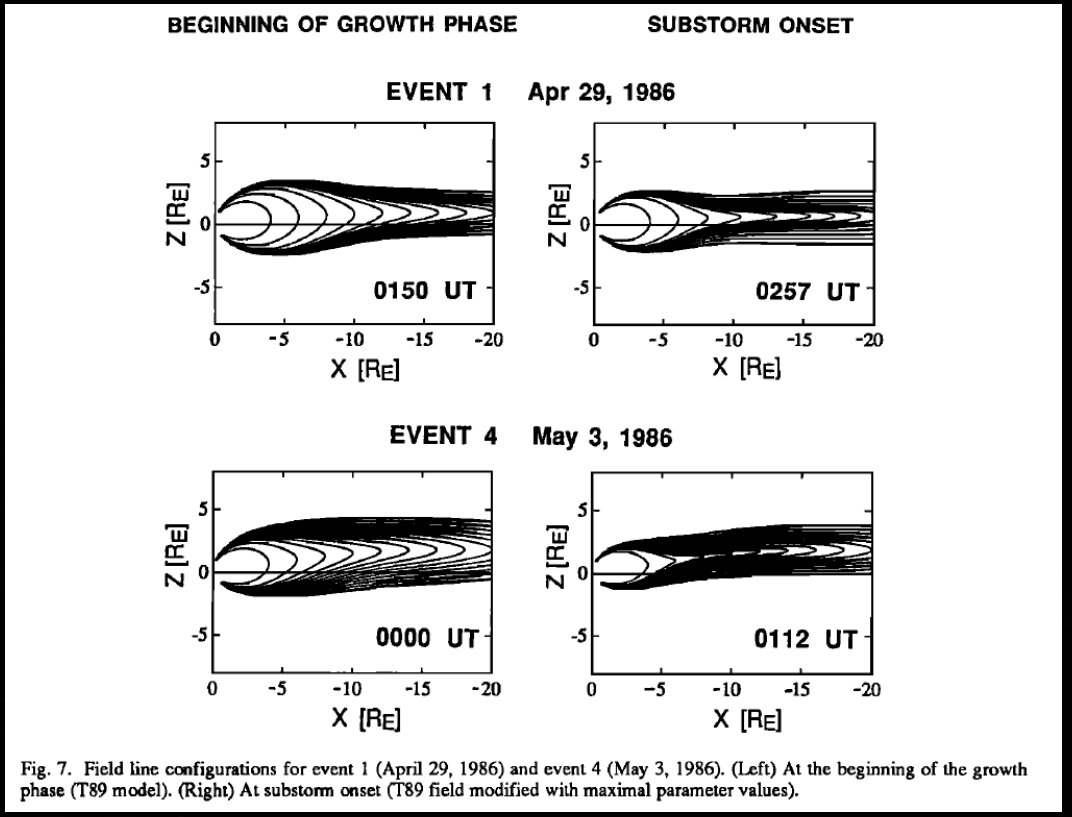

Fig. 7. Field line configurations for event 1 (April 29, 1986) and event 4 (May 3, 1986). (Left) At the beginning of the growth phase (T89 model). (Right) At substorm onset (T89 field modified with maximal parameter values).

Pulkkinen *et al.*, *J. Geophys. Res.*, 97, A12, 19283, 1992.

Growth-Phase Modeling

Kappa values (regions of chaotic behavior).

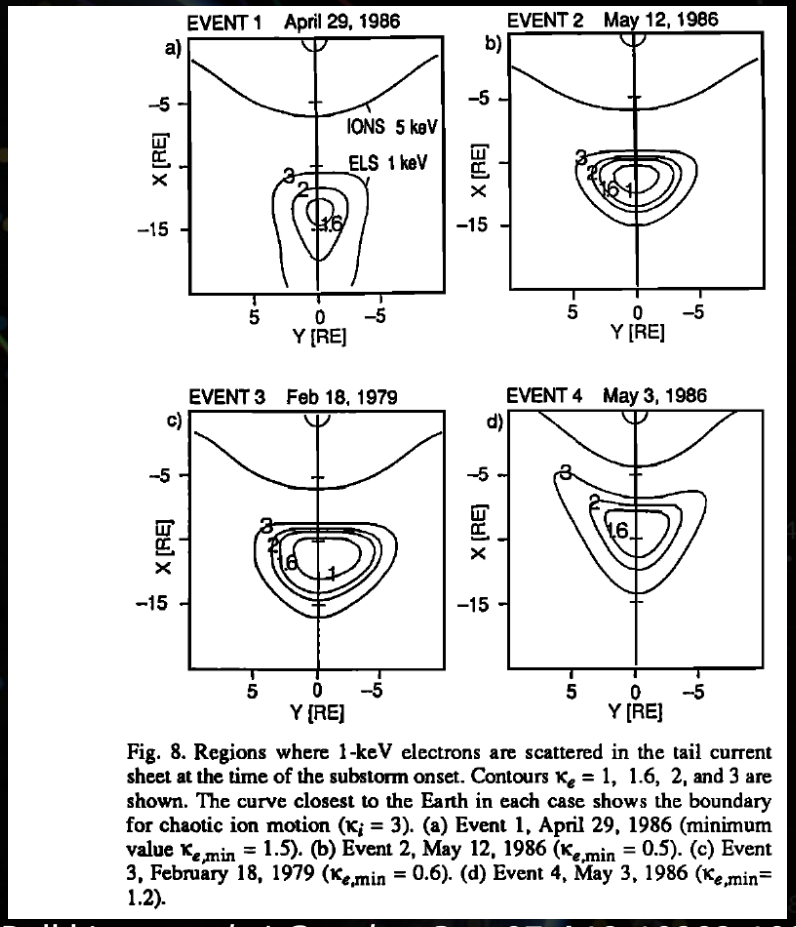

Fig. 8. Regions where 1-keV electrons are scattered in the tail current sheet at the time of the substorm onset. Contours κ_e = 1, 1.6, 2, and 3 are shown. The curve closest to the Earth in each case shows the boundary for chaotic ion motion (κ_i = 3). (a) Event 1, April 29, 1986 (minimum value $\kappa_{e,min}$ = 1.5). (b) Event 2, May 12, 1986 ($\kappa_{e,min}$ = 0.5). (c) Event 3, February 18, 1979 ($\kappa_{e,min}$ = 0.6). (d) Event 4, May 3, 1986 ($\kappa_{e,min}$= 1.2).

Pulkkinen *et al.*, *J. Geophys. Res.*, 97, A12, 19283, 1992.

Comparison of ASC growth phase arc locations with mapped regions of non-adiabatic behavior

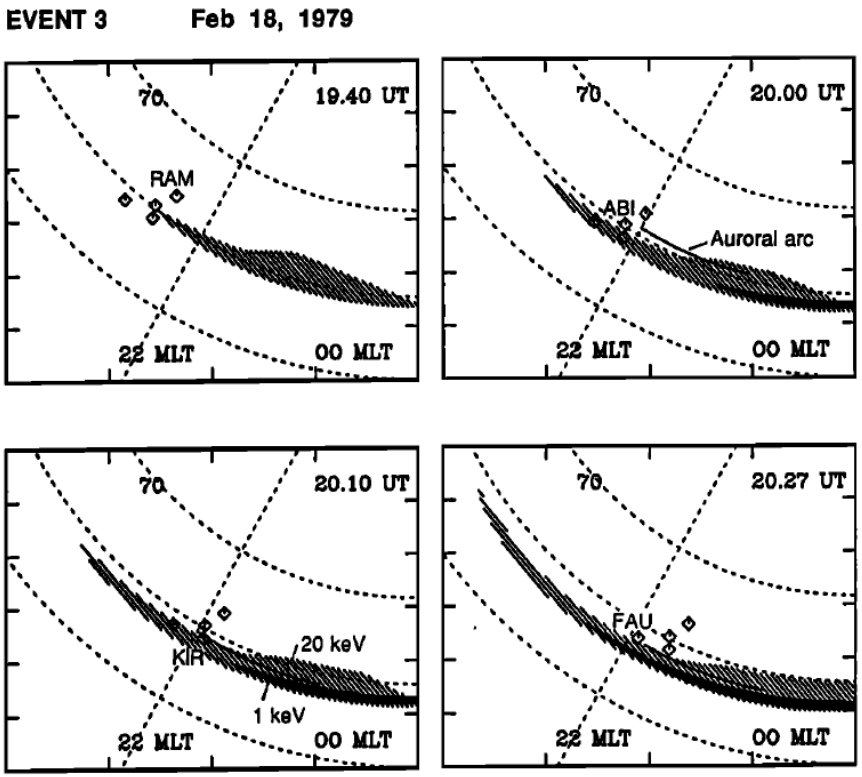

Fig. 10. Location of the growth phase auroral arc obtained from all-sky camera observations (thin solid line), the location of the riometer absorption maximum (at riometer station (diamonds) named in each frame), and the ionospheric mapping of the equatorial current sheet region where the electron motion is nonadiabatic (1-keV electrons shown in solid, 20-keV electrons shown hatched) at 1940 UT, 2000 UT, 2010 UT, and 2027 UT on February 18, 1979.

Pulkkinen *et al.*, *J. Geophys. Res.*, 97, A12, 19283, 1992.

Other Studies

- Sergeev *et al.*, Hybrid state of the tail magnetic configuration during steady convection events, *J. Geophys. Res.*, 99, A12, 23571, 1994.

  Added additional ring current term to T89 model.

- Ganushkina *et al.*, Event-oriented modelling of magnetic fields and currents during storms, *Adv. Polar Upper Atmos. Res.*, 18, 105, 2004.

  Heavily modified T89 model. Ring current term replaced with `bean-shaped' current system. Partial RC with region 2 FACs added. A new thin tail current sheet was added and many of the parameters were made adjustable and fit to data.

- Kubyshkina *et al.*, Magnetospheric currents during sawtooth events, J. *Geophys. Res.*, 113, A08211, doi:10.1029/2007JA012983, 2008.

  Comparison of 3 different approaches: 1) the Ganushkina [2004] modeling approach; 2) event-fitted input parameters for the T01s model; 3) Modified T96 model (added current terms and several adjustable free parameters) fit to data. April 18 2002 sawtooth event reasonably well modeled. BUT, mapping "... from the ionosphere to the magnetotail along magnetic field lines still not very accurate at times."

Other Metrics for Optimization

- A best match to the observed B-field has not been the only criterion used to select the best model.
- Chen *et al.*, *J. Geophys. Res.*, 112, A11214, doi:10.1029/2007JA012314.

  Used a Phase Space Density (PSD) matching approach to select the best model from many available models.

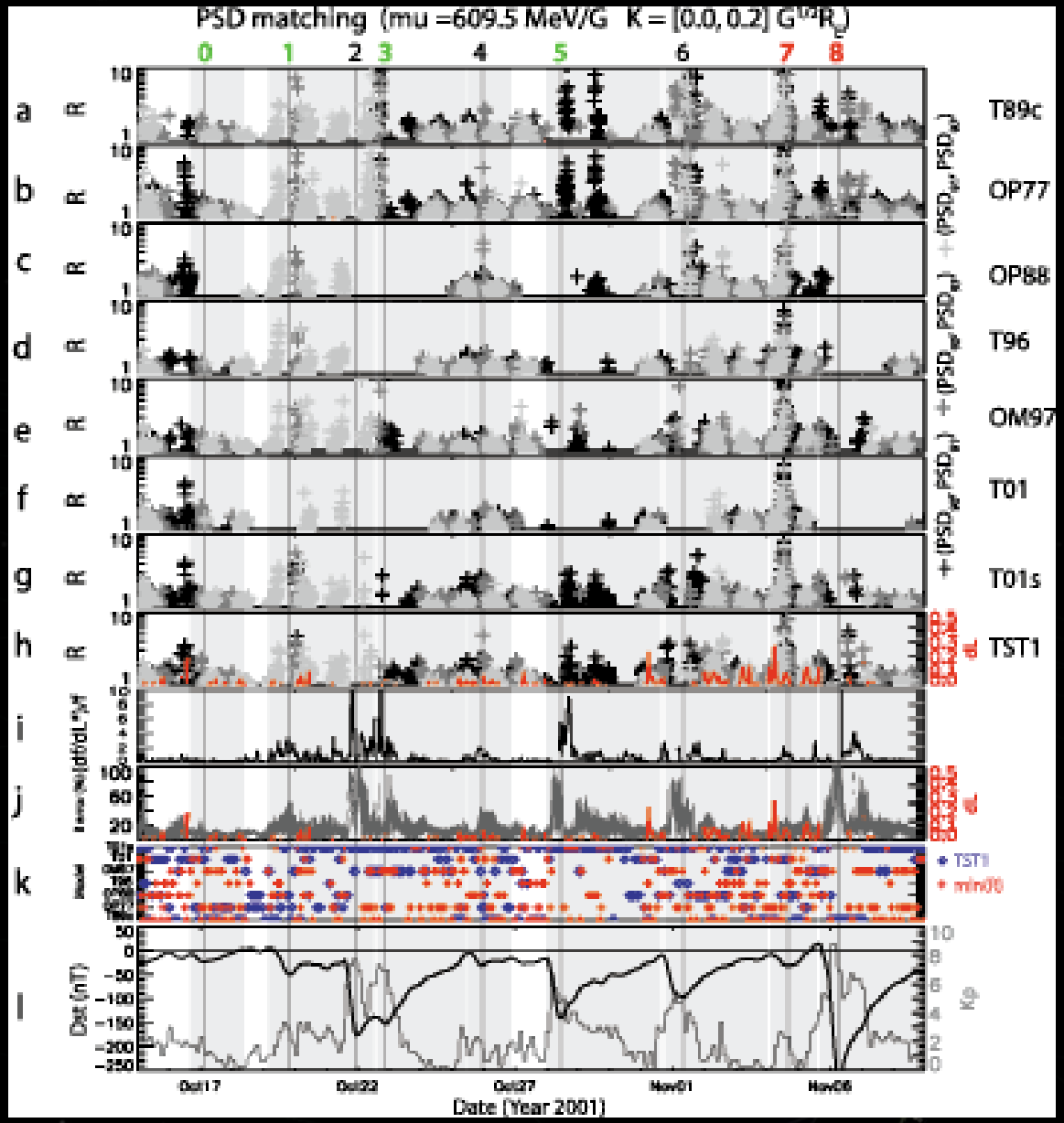

How Can we do Better?

- Use additional observational constraints. For example make use of;
  - Mapping constraints like the location of the open/closed boundary at high latitudes and the location of the isotropic boundaries at low latitudes. Others?
  - Observed magnetopause location.
  - PSD observations (e.g. at GEO, GPS, THEMIS, RBSP, etc.)
  - Stable/Quasi-Trapping boundaries and magnetopause shadowing observations.
  - ENA imagery. (Not clear how to make use of them, but modeling them depends on B).
- Add more physically appropriate currents systems. E.g. time-dependent substorm current wedges. Plasmoids? Flux ropes?
- Make more of the parameters adjustable.
- Utilize *a-priori* constraints (may be necessary to regularize problem). For example;
  - Smoothness constraints.
  - Ensure no x-lines too close to Earth.
  - Constraints on force balance and/or profile of PV^{γ}
  - Others?

Stable and Quasi-Trapping Regions

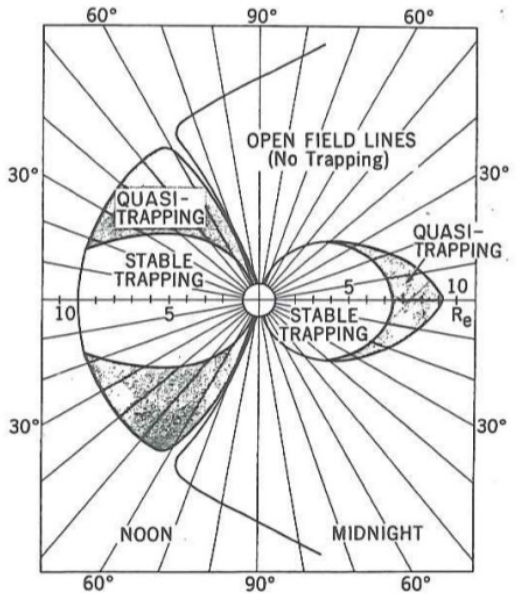

Fig. 51. Location of the quasi-trapping regions in the magnetosphere [*14*]. Particles mirroring inside those regions are unable to complete a 360° drift around the earth. Those injected into the left side will be lost into the tail; those injected into the right portion will abandon the magnetosphere through the boundary on the dayside

- Particles unable to execute full drift orbits are quasi-trapped.

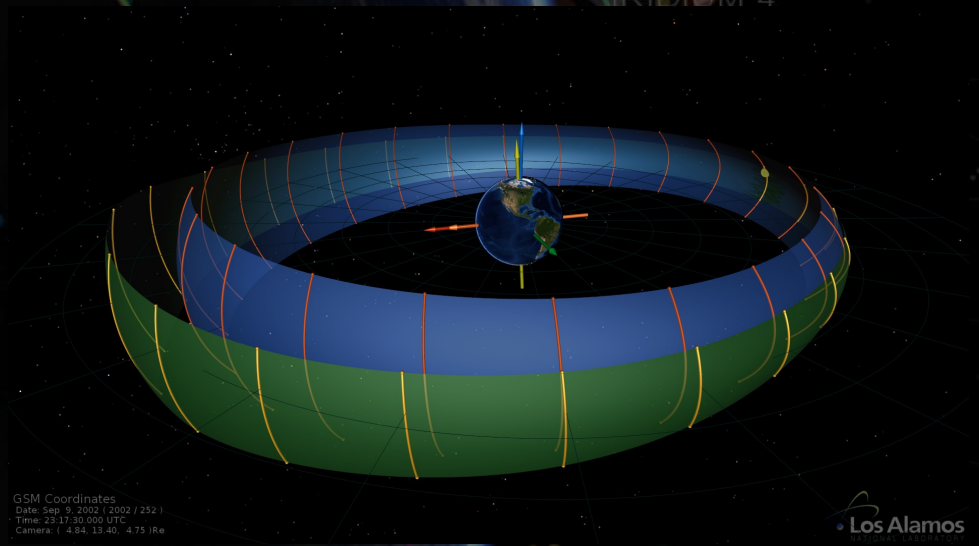

- E.g., magnetopause shadowing leads to pitch angle dependent losses. Can we use magnetopause shadowing results to constrain models?

Los Alamos
NATIONAL LABORATORY

Constraints From UBK Analysis?

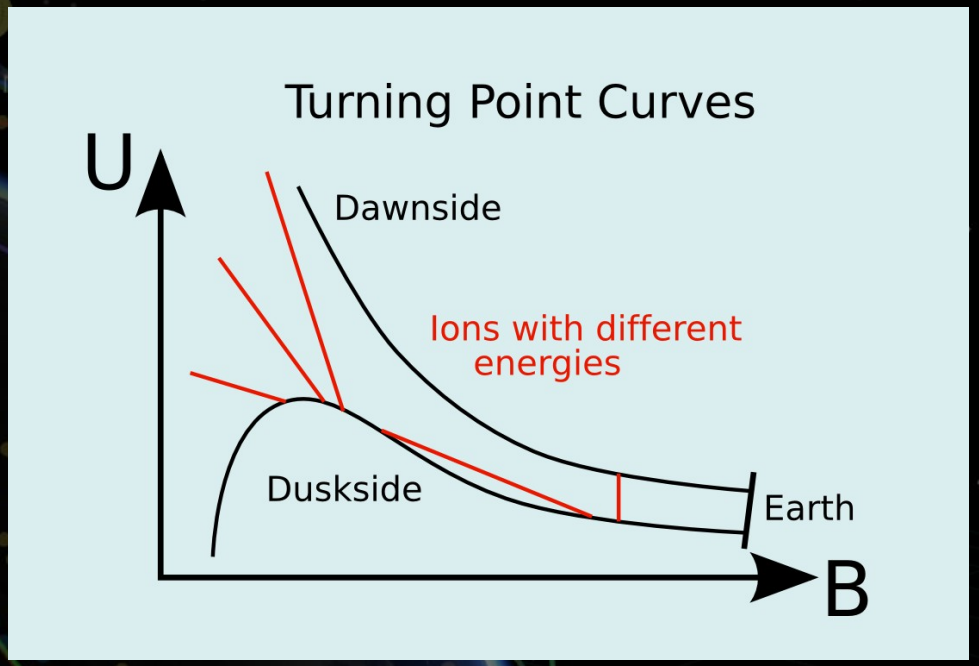

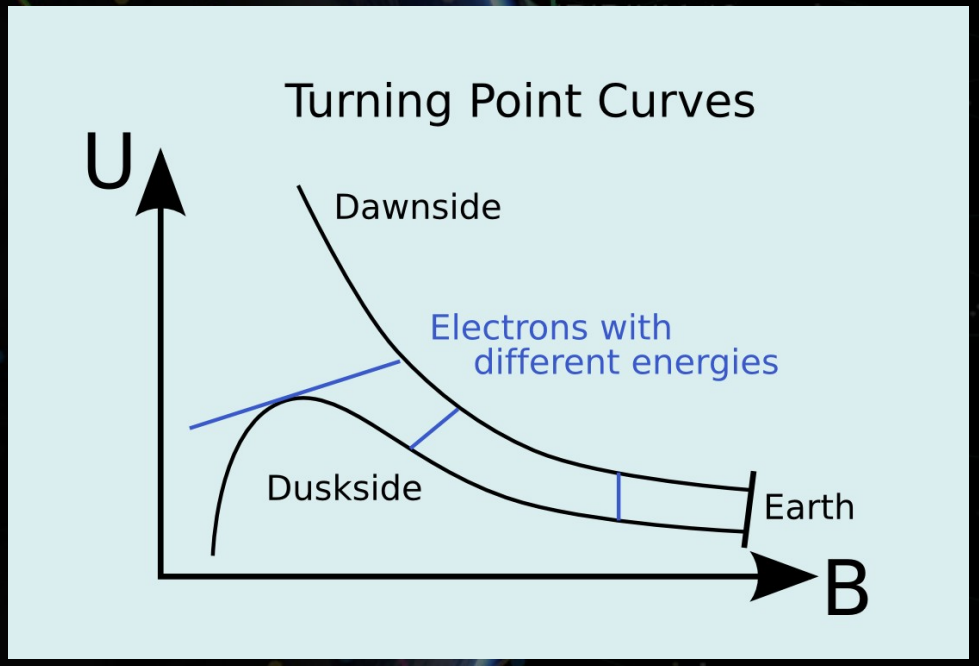

Access of lower energy particles to inner magnetosphere could also be used to constrain B-field models (via UBK analysis), but proper specification of E-field would be needed also.

This approach might be useful when both E- and B-field models are optimized simultaneously.

Mapping with Model Fields

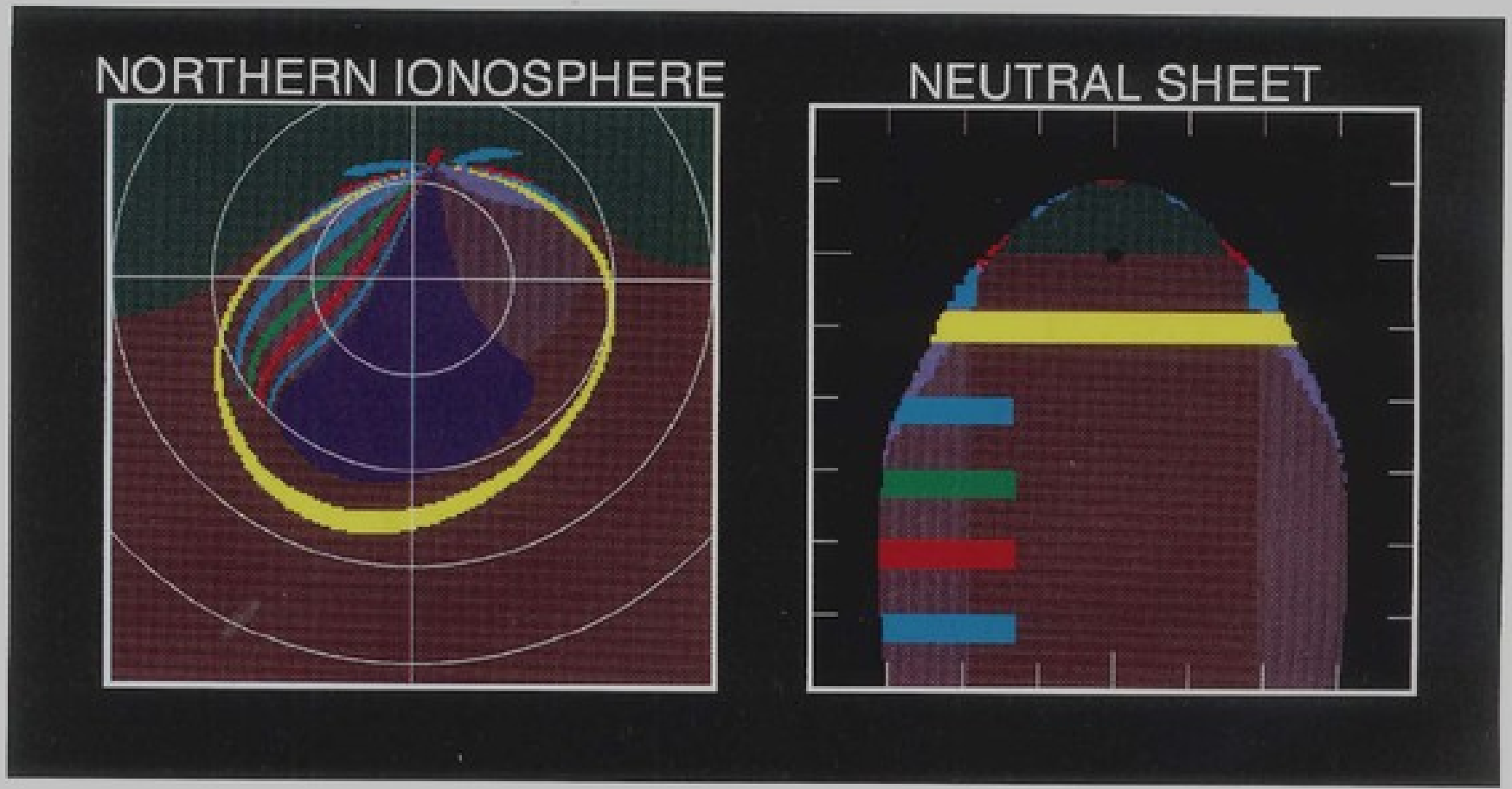

Figure 8.9: Magnetospheric mapping in the T87 model. The yellow regions in the neutral sheet map roughly to the auroral oval. The blue and red regions sunward of the yellow line also contribute to the (dayside) oval. The blue, green and red lines anti-sunward of the yellow line map to high-latitude duskside arcs (a similar mapping also occurs on the dawn side to produce fan arcs). Missing pixels in the neutral sheet (i.e. pixels that had no field lines passing through them) were filled in using a boundary-finding algorithm.

Topology of Model Fields - T87

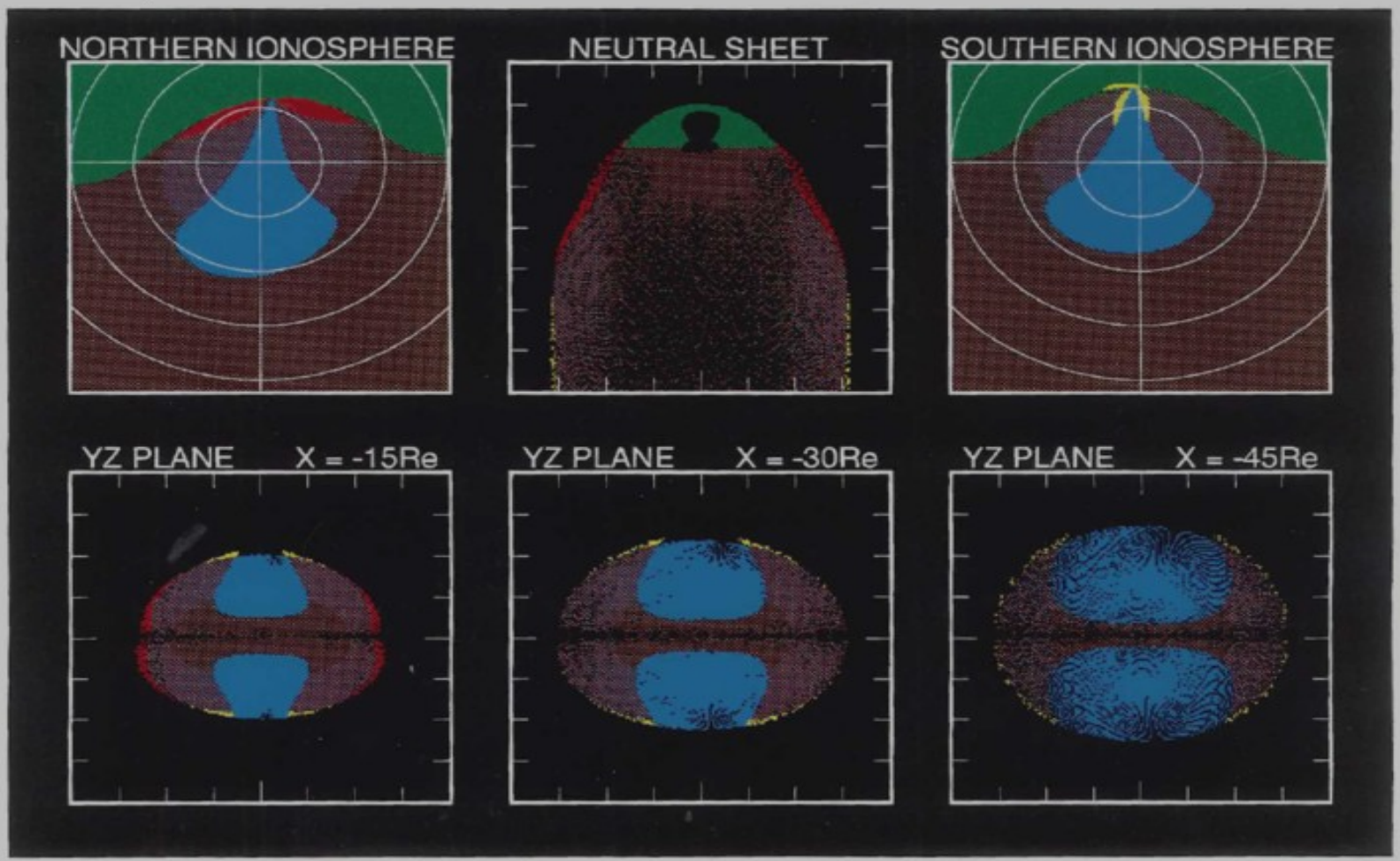

Figure 8.7: Magnetospheric mapping of field lines in the T87 Long model for $K_p = 2$ and $\psi = 5°$.

Topology of Model Fields -T89

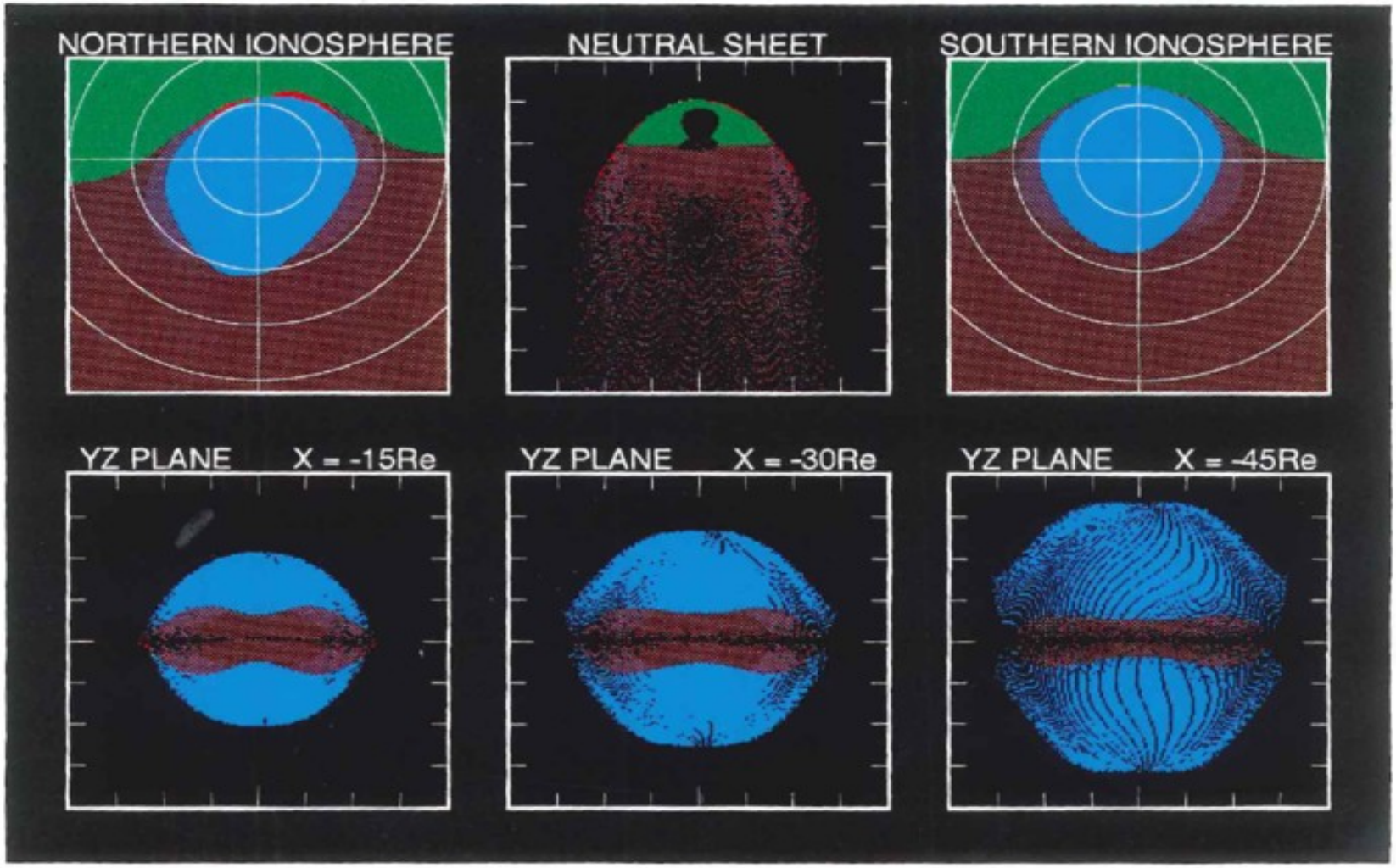

Figure 8.8: Magnetospheric mapping of field lines in the T89 model for $K_p = 2$ and $\psi = 5°$.